

Ballistic spin transport in a two-dimensional electron gas

H. X. Tang, F. G. Monzon, Ron Lifshitz, M. C. Cross, and M. L. Roukes*

Condensed Matter Physics 114-36, California Institute of Technology, Pasadena, California 91125

(Received 28 July 1999)

We explore electrically injected, spin-polarized transport in a ballistic two-dimensional electron gas. We augment the Büttiker-Landauer picture with a simple, but realistic model for spin-selective contacts to describe multimode reservoir-to-reservoir transport of ballistic spin-1/2 particles. Clear and unambiguous signatures of spin transport are established in this regime, for the simplest measurement configuration that demonstrates them directly. These effects originate from spin precession of ballistic carriers; they exhibit a strong dependence upon device geometry, and vanish in the diffusive limit. Our results have important implications for prospective “spin transistor” devices.

The concept of a spin transistor, first proposed almost ten years ago,¹ has attracted widespread interest² but its experimental realization remains elusive.³ It is based upon electrical injection of spin-polarized carriers from a ferromagnetic conductor into an electron gas within a semiconductor. Electrons propagating in the interfacial electric field confining them to the device channel experience an effective magnetic field that induces spin precession; this is called the Rashba effect.⁴ The rate of spin precession should be tunable through an external gate voltage, which will add to the confinement potential.^{5,6} With ferromagnetic source and drain contacts acting as spin polarizer and analyzer, an electron device analogous to an electro-optic modulator⁷ is envisaged.

Experiments to date demonstrate that the spin transistor geometry [Fig. 1(a)], in general, leads to strong Hall phenomena that are unrelated to true spin transport.⁵ They arise due to the requisite proximity of miniature magnets and the low density (and, hence, high Hall coefficient) electron gas. Since these Hall phenomena depend directly upon the magnetization state of these magnetic contacts, they often closely mimic the signals expected from spin transport experiments—especially those in which the relative magnetic orientation of the “spin polarizer” and “analyzer” contacts is varied. However, in early experiments on (diffusive) spin injection in metals,⁸ spin precession phenomena provided an alternate and crucial experimental proof of spin transport. In this paper, we establish analogous, and unambiguous, experimental signatures to be expected from spin injection and precession phenomena in a ballistic two-dimensional electron gas (2DEG). The observation of these precessional effects will constitute a definitive experimental demonstration of electrical spin injection in semiconductor systems.

The spin transresistance, R_S [Fig. 1(a)] provides the most direct demonstration of spin transport.⁸ This nonlocal transport coefficient is free of obfuscating background signals unrelated to spin injection. In the *diffusive* limit, if current contact **F1** is replaced with one that is unpolarized, no voltage will appear between the analyzer contact **F2** and a suitably defined ground reference **R**. In this case these voltage contacts, being well outside the net current path, remain at equipotential. With a polarized current contact **F1**, injected magnetization can lead to steady-state *spin accumulation* that

persists over the entire length of the channel if $\delta_S \geq L$. This induces disequilibrium between the electrochemical potentials of **F2** and **R**, and yields a finite R_S . Here $\delta_S = \sqrt{l_0 l_S/2}$ is the spin diffusion length, $l_S = v_F \tau_S$ and $l_0 = v_F \tau_0$ are the spin and momentum mean free paths, τ_S and τ_0 are the effective spin and momentum relaxation times, and v_F is the Fermi velocity.

In the *ballistic* regime, however, it is not appropriate to speak of spin accumulation since a local chemical potential cannot be meaningfully defined within the channel. Accord-

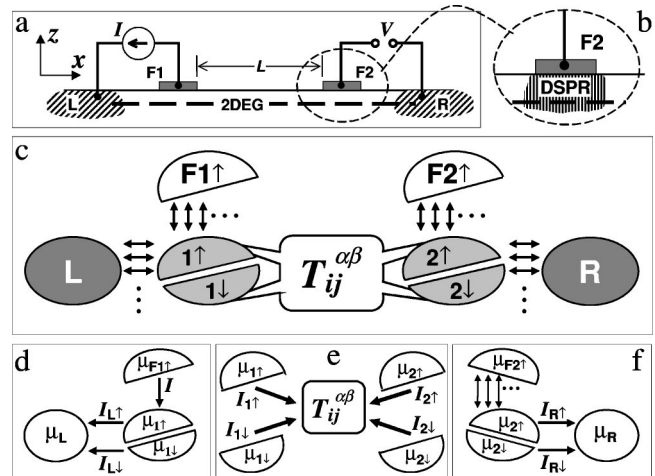


FIG. 1. Model for ballistic spin injection in two dimensions. (a) Measurement configuration: a current I is injected through the 2DEG via a ferromagnetic contact **F1** and an Ohmic contact **L**. The spin transresistance $R_S = V/I$ arises from spin-polarized carriers traversing a distance L from the net path of the current, which induce a nonlocal voltage, V , between a second, similar, pair of contacts **F2** and **R**. (b) The conductor beneath the ferromagnetic contacts (DSPR) is assumed to be a *disordered, but spin preserving region*. (c) The full eight-reservoir model; complete ellipses represent spin-relaxing reservoirs, and half ellipses represent spin-resolved reservoirs. **F1** and **L** are current contacts, **F2** and **R** are voltage probes. $T_{ij}^{\alpha\beta}$ denotes the 2DEG device channel in which spin precession occurs. Other multimode leads are denoted by three arrows and ellipsis. Panels (d), (e), and (f) illustrate decomposition of the eight-reservoir model. [Panel (e) depicts the reduced four-reservoir problem.]

ingly, our description of the ballistic spin transresistance is based upon Büttiker's picture for mesoscopic transport within a multiprobe conductor.⁹ Here we augment this with a model describing spin-selective contacts. Our procedure is as follows: (a) We first develop a simple description of spin-selective contacts, based upon careful consideration of the ferromagnetic/semiconductor (F/S) contacts in (our) real devices.³ (b) We construct an eight-reservoir model, after Büttiker, to describe the spin injection experiment. (c) Boundary conditions are used to constrain the spin-resolved currents and chemical potentials. These lead to a simpler four-reservoir problem for the spin transresistance, R_S , in terms of reservoir-to-reservoir, *spin-resolved* transmission probabilities, $T_{ij}^{\alpha\beta}$, of the 2DEG forming the device conduction channel. Here the indices i and j specify the reservoirs themselves, and α and β their constituent spin bands. (d) The requisite $T_{ij}^{\alpha\beta}$ are then calculated semiclassically, using a modified Monte Carlo numerical technique (described below). We follow the electrons' ballistic trajectories *and* the phase of their spin wave functions as they pass through the device, while ignoring the phase of their spatial wave functions. For unpolarized ballistic systems, this semiclassical approach has proven remarkably consistent with experimental data at $T \sim 4$ K, where the electron phase coherence length is smaller than typical dimensions of nanoscale devices.¹⁰

Figure 1(b) depicts our model for the spin-selective contacts which comprises two elements: **F2**, a fully spin-polarized reservoir which is in perfect contact with a second *disordered* (i.e., momentum-randomizing) but *spin-preserving region* (DSPR) that consists of separate spin-up and spin-down bands. The separate spin-resolved reservoirs comprising the DSPR's ($1\uparrow, 1\downarrow, 2\uparrow, 2\downarrow$) model low-mobility regions always present beneath unalloyed ferromagnetic metal contacts in typical InAs devices.³ Disorder within them yields significant momentum randomization and, hence, a short l_0 . However, in contrast to the usual picture describing unpolarized reservoirs,⁹ we assume these special contacts are small compared to δ_S , thus any spin disequilibrium within them is preserved. This, in fact, is consistent with the more restrictive constraint $\delta_S \geq L$, which is generic and fundamental to any spin injection experiment. If significant spin relaxation occurs anywhere in the device, including the vicinity of the ferromagnetic contacts, spin-selective transport is suppressed.¹¹ In this paper, for sake of clarity, we consider the most ideal situation, initially assuming that **F1** and **F2** are fully polarized at the Fermi surface (half-metals). This approximation serves to illustrate the most important aspects of the underlying physics. Of course, many complexities in real devices may diminish spin transport effects.¹² Here our aim is to establish what may be expected in ballistic systems under *optimal* conditions.

Measurement of R_S involves four terminals [Fig. 1(a)], two that are spin selective, **F1** and **F2**, and two that are conventional, i.e., momentum- and spin-relaxing, **L** and **R**. As depicted in Figs. 1(d)–1(f), the full problem separates into three sub components. Figure 1(d) represents the spin-up and spin-down currents ($I_{L\uparrow}, I_{L\downarrow}$) that flow between **F1**, $1\uparrow, 1\downarrow$, and **L**. A Sharvin resistance,¹³

$$R_{sh} = (h/2e^2)(k_F w) / \pi = (h/2e^2)N_{ch}$$

arises between $1\uparrow, 1\downarrow$, and the multichannel conductors connecting them to **L**. Under conditions of current flow this yields the spin-resolved electrochemical potential differences $\mu_{1\uparrow} - \mu_L = 2eR_{sh}I_{L\uparrow}$ and $\mu_{1\downarrow} - \mu_L = 2eR_{sh}I_{L\downarrow}$. Here the factors of 2 arise because transport is spin resolved; k_F , w , and N_{ch} are the Fermi wave vector, channel width, and number of occupied modes within the 2DEG device channel, respectively. Similarly, at the rightmost side of Fig. 1(f), current flow between the reservoirs $2\uparrow, 2\downarrow$, and **R** establishes the electrochemical potential differences $\mu_{2\uparrow} - \mu_R = 2eR_{sh}I_{R\uparrow}$ and $\mu_{2\downarrow} - \mu_R = 2eR_{sh}I_{R\downarrow}$. Also, $\mu_{F2\uparrow} = \mu_{2\uparrow}$ since no current flows between these reservoirs. Note that all I 's here represent *net* currents (forward minus reverse contributions). In our model, the following sum rules hold: $I = I_{L\uparrow} + I_{1\uparrow}$, $I = I_{L\downarrow} + I_{1\downarrow}$, $0 = I_{R\uparrow} + I_{R\downarrow}$, and $I_{1\uparrow} + I_{1\downarrow} = I_{2\uparrow} + I_{2\downarrow} = 0$. As the reservoirs in Fig. 1(f) are voltage contacts, net current is conserved separately for each spin band, $I_{R\uparrow} + I_{2\uparrow} = I_{R\downarrow} + I_{2\downarrow} = 0$. These expressions can be manipulated to yield

$$\begin{pmatrix} \mu_{1\uparrow} \\ \mu_{1\downarrow} \\ \mu_{2\uparrow} \\ \mu_{2\downarrow} \end{pmatrix} = \begin{pmatrix} \mu_L + 2eR_{sh}(I - I_{1\uparrow}) \\ \mu_L + 2eR_{sh}I_{1\uparrow} \\ \mu_R - 2eR_{sh}I_{2\uparrow} \\ \mu_R + 2eR_{sh}I_{2\uparrow} \end{pmatrix}. \quad (1)$$

Given these relations, calculation of R_S reduces to a four-terminal problem that solely involves the four spin-resolved reservoirs $1\uparrow, 1\downarrow, 2\uparrow$, and $2\downarrow$ and the 2DEG device channel that connects them [Fig. 1(e)]. Modifying Büttiker's formula to account for the spin-resolved channels, the four-terminal linear response at zero temperature becomes

$$I_{i\alpha} = \frac{e}{h} [(N_{ch} - R_{ii}^{\alpha\alpha})\mu_{i\alpha} - T_{ij}^{\alpha\beta}\mu_{j\beta}] \equiv \frac{e}{h} U_{ij}^{\alpha\beta}\mu_{j\beta}. \quad (2)$$

Transport within the ballistic multimode 2DEG conductor is fully represented by the transmission and reflection coefficients $T_{ij}^{\alpha\beta}$ and $R_{ii}^{\alpha\alpha}$. These describe carriers incident from the lead i with spin polarization α , that are transmitted into lead j with final spin state β ; and carriers incident from $i\alpha$ that are reflected back into same lead and spin channel, respectively. The coefficients U_{ij} in Eq. (2) satisfy the sum rule $\sum_{i\alpha} U_{ij}^{\alpha\beta} = \sum_{j\beta} U_{ij}^{\alpha\beta} = 0$, ensuring the current sum rules of Eq. (1), and that all currents vanish when the μ_i are equal.

Simplification of Eqs. (1) and (2) yields

$$\begin{pmatrix} I_{1\uparrow} \\ I_{1\downarrow} \\ I_{2\uparrow} \\ I_{2\downarrow} \end{pmatrix} = S \begin{pmatrix} \tilde{\mu}_L + I \\ \tilde{\mu}_L \\ \tilde{\mu}_R \\ \tilde{\mu}_R \end{pmatrix}, \quad (3)$$

where $\tilde{\mu}_{L,R} = \mu_{L,R}/2eR_{sh}$ and $S \equiv (1 + U)^{-1}U$. The elements of S satisfy the same sum rules that constrain U (for identical reasons). For parallel alignment of polarizer and analyzer, **F1** and **F2**, which we denote by the superscript ($\uparrow\uparrow$), these steps yield

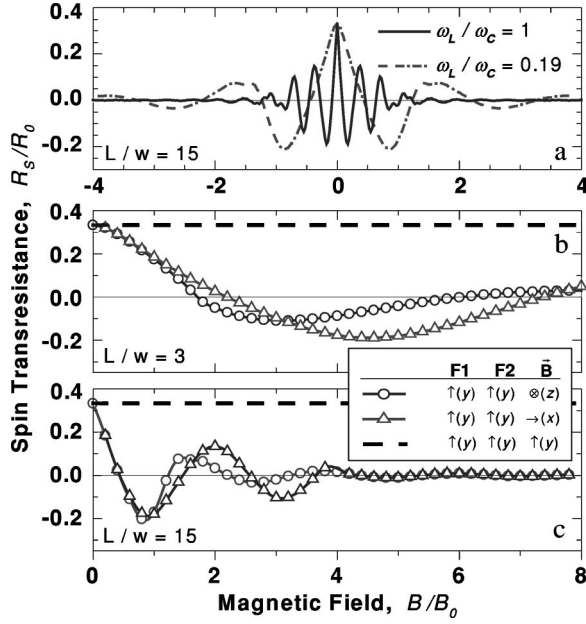


FIG. 2. Ballistic spin transresistance in an external field normalized to $B_0 = p_F/e w$, at which the cyclotron radius equals the channel width. (a) For a channel with $L/w = 15$ in a perpendicular field, we plot two traces representing $\omega_L/\omega_c = 1$ and 0.19 , appropriate for a typical metal and for InAs, respectively. (b) and (c) Spin transresistance for three different configurations and two channel lengths $L/w = 3$ and 15 . Here $\omega_L/\omega_c = 0.19$ (InAs).

$$R_S^{(\uparrow\uparrow)} = -2 \frac{S_{31}S_{42} - S_{32}S_{41}}{S_{31} + S_{32} + S_{41} + S_{42}} R_{sh}. \quad (4)$$

For antiparallel alignment, only the sign changes: $R_S^{(\uparrow\downarrow)} = -R_S^{(\uparrow\uparrow)}$.

We obtain the requisite elements of S numerically, extending the semiclassical billiard model¹⁰ to allow tracking of an electron's spin wave function along ballistic trajectories linking the spin-resolved reservoirs ($1\uparrow, 1\downarrow, 2\uparrow, 2\downarrow$) at either end of the 2DEG device channel. We consider electrons confined within a hard-wall channel, of length L and width w . $T_{ij}^{\alpha\beta}$ are calculated by injecting and following a large number of electron trajectories (typically $> 10^4$) propagating at v_F .¹⁴

For each path segment traversed by the electron between boundary reflections, the phase of its spin wave function evolves continuously via the local Larmor frequency $\omega_L = g^*eB/2m$. Here g^* is the effective electron g factor, B the local magnetic field, and m the free-electron mass. Total precession is accumulated for each complete trajectory, which is the sum of these segments. For each segment the electron's spin precession is calculated analytically¹⁵ and incorporated into the Monte Carlo procedure.

In Fig. 2(a) we display $R_S^{(\uparrow\uparrow)}$ as a function of perpendicular magnetic field strength. The prominent feature is that R_S is *oscillatory*, a ballistic phenomenon not found in the diffusive regime. In Figs. 2(b) and 2(c), we display $R_S^{(\uparrow\uparrow)}$ calculated for three orientations of the external field—two that are in plane and the perpendicular case, displayed again for comparison. In all three cases the **F1** and **F2** magnetizations are parallel and \hat{y} -oriented.

When the external field is along \hat{y} , the injected carriers remain in spin eigenstates and do not precess. In this situation $R_S^{(\uparrow\uparrow)}$ is a positive constant [Figs. 2(b) and 2(c)]. However, with an \hat{x} -oriented field, precession is maximal, and R_S oscillates. Since orbital effects are absent for an in-plane field, the oscillations in this case arise purely from spin precession, and the oscillation *period*, ΔB is determined by the condition $2\pi n = \omega_L t_{TR}$, i.e., $\Delta B = h/(g^* \mu_B t_{TR})$. Here $t_{TR} = S/v_F$ is a typical transit time from $1 \rightarrow 2$, and μ_B is the electronic Bohr magneton. ΔB is thus inversely proportional to S , a typical path length averaged over the injection distribution function. The *decay* of R_S occurs on a field scale where $\omega_L \delta t_{TR} \sim \pi$; i.e., for $B = \hbar \pi / (g^* \mu_B \delta t_{TR})$, beyond which precession among the different contributing trajectories tends to get out of step. Here $\delta t_{TR} = [t_{TR}^2 - \langle t_{TR}^2 \rangle]^{1/2}$ is the variance in path lengths traversed while propagating from $1 \rightarrow 2$.

The perpendicular field ($B_{ext} \parallel \hat{z}$) is special—it induces both spin and *orbital* effects. (The characteristic field scale for the latter is $B_0 = p_F/e w$ at which the cyclotron radius $r_c = v_F/\omega_c$ equals the channel width w .) The frequency ratio $\omega_L/\omega_c = (g^*/2)(m^*/m)$ describes the relative importance of orbital and spin transport phenomena. Here p_F is the Fermi momentum, $\omega_c = eB/m^*$ the cyclotron frequency, and m^* the effective mass. For InAs ($m^* = 0.025$, $g^* = 15$) this ratio is ~ 0.19 , for $\text{In}_x\text{Ga}_{1-x}\text{As} \sim 0.1$, whereas it is roughly 1.0 for most metals. In the latter spin and orbital effects have similar periodicity so disentangling them is difficult [Fig. 2(a)].

As mentioned, electrons confined within an InAs heterostructure are subject to an internal Rashba field, present even for zero applied magnetic field. This can be modeled by a Hamiltonian,⁴ $H_R = \alpha_{so}[\boldsymbol{\sigma} \times \mathbf{k}] \cdot \hat{z}$. Comparing H_R to the Zeeman term we write the effective Rashba field as $\mathbf{B}_R = 2\alpha_{so}\mathbf{k} \times \hat{z} / (g^* \mu_B)$. Here $\alpha_{so} = \Delta_R/2k_F$ is the spin-orbit coupling parameter (Δ_R is the Rashba splitting,¹⁶) and \mathbf{k} and k_F are the electron and Fermi wave vectors, respectively. Using data from Heida *et al.*,¹⁶ we estimate this internal field to be about 5 T for an InAs 2DEG. Since \mathbf{B}_R is always in plane, all electron trajectories are straight when the external field has no out-of-plane component. For fully polarized injection, this yields the simple expression

$$R_S^{(\uparrow\uparrow)} = \frac{1 - 2t}{(1 + 2t)(2t - 3)} R_{sh}, \quad (5)$$

where t represents $T_{(1\uparrow \rightarrow 2\uparrow)}$, normalized by N_{ch} .

Figure 3 displays how Rashba-induced spin precession is manifested in R_S for a zero external field. We represent the effective Rashba field strength by the dimensionless frequency $\hat{\omega}_R = 2\alpha_{so}m^*w/\hbar^2$; at $\hat{\omega}_R = 1$ an electron precesses 1 rad after traversing a distance w . As shown, the oscillations decay quickly initially, but exceedingly slowly thereafter. No spin precession occurs for $\hat{\omega}_R = 0$; hence $t = 1$ yielding $R_S^{(\uparrow\uparrow)} = R_S^{(\rightarrow\rightarrow)} = R_{sh}/3$, a simple result of current division. For finite $\hat{\omega}_R$, R_S displays strong dependence upon the orientation of the magnetizations \mathbf{M} (of **F1** and **F2**; assumed parallel), in relation to the device channel's principal axis (\hat{x}). For $\mathbf{M} \parallel \hat{x}$ (parallel to the channel), precessional effects are maximal. With increasing Rashba field, the variance in con-

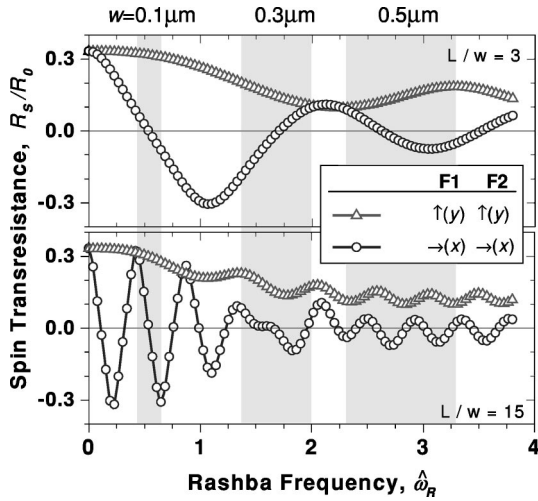


FIG. 3. Spin transresistance vs reduced Rashba frequency $\hat{\omega}_R = 2m^*\alpha_{so}w/\hbar^2$, at zero applied (external) field, for two different device channel lengths $L/w=3$ and 15 . The parameter $\hat{\omega}_R$ can be controlled by an external gate voltage. Shaded regions delineate the range of tunability expected for $\text{In}_x\text{Ga}_{1-x}\text{As}$ devices (Ref. 5) of three widths, 0.1 , 0.3 , and $0.5 \mu\text{m}$.

tributing path lengths causes the oscillations in R_S to decay, as described previously for the case of finite external field. Here, however, the contributions from short paths (direct propagation between the DSPR's involving few or no boundary reflections) continue to add coherently for large $\hat{\omega}_R$, resulting in very slow decay. For $\mathbf{M}||\hat{y}$ most of the injected carriers experience a Rashba field nearly aligned with their spin. At intermediate Rashba field these yield small oscillations that center about a *finite* value of R_S . The other carriers

make a contribution to R_S at small $\hat{\omega}_R$, but this becomes incoherent, and thus quickly decays for large $\hat{\omega}_R$.^{11,17}

The original idea of the spin transistor involved use of an external gate potential, acting in concert with the intrinsic confinement potential, to control of the spin precession rate.¹ We note, however, that gate tuning of Δ_{so} for electrons has been experimentally demonstrated in relatively few narrow-gap semiconductor heterostructures. Two such systems are $\text{In}_x\text{Ga}_{1-x}\text{As}/\text{InP}$ and $\text{In}_x\text{Ga}_{1-x}\text{As}/\text{In}_x\text{Al}_{1-x}\text{As}$.^{5,6} In the latter, tuning over about a 30% range has been reported. In Fig. 3 we show how this range of tunability translates into a direct modulation of R_S , for three device widths. Our calculations clearly illustrate that the ‘‘conventional’’ spin transistor configuration, $\mathbf{M}||\hat{y}$, (which is most easily fabricated) is *not* optimal—even for a very short channel ($L \sim l_S$). We find that tunability is maximized for $\mathbf{M}||\hat{x}$.

The spin transistor was originally envisaged as a one-dimensional device, with only a single populated transverse subband. Realizable devices in the near term will more likely be two-dimensional or, perhaps, quasi-one-dimensional, channels. Their increased phase space for scattering can lead to quick suppression of R_S , especially in the presence of moderate scattering.¹¹ Hence it appears that an extremely narrow channel is a basic requirement for a spin transistor.

Our calculations of R_S clarify the important, and unique, signatures of spin-injected transport in an electron gas within a semiconductor. They also point out crucial experimental challenges that must be faced in making a spin transistor.

We gratefully acknowledge support from DARPA Spintronics, through ONR Grant No. N00014-96-1-0865. We also thank A. Polichtchouk and M. Hartl for contributions to this work.

*Electronic address: roukes@caltech.edu

¹S. Datta and B. Das, Appl. Phys. Lett. **6**, 665 (1990).

²See, e.g., G.A. Prinz, Phys. Today **48**(4), 58 (1995).

³F.G. Monzon and M.L. Roukes (unpublished); F.G. Monzon, Ph.D. thesis, Caltech, 1999.

⁴E.I. Rashba, Fiz. Tverd. Tela (Leningrad) **2**, 1224 (1960) [Sov. Phys. Solid State **2**, 1109 (1960)].

⁵J. Nitta, T. Akazaki, and H. Takayanagi, Phys. Rev. Lett. **78**, 1335 (1997).

⁶G. Engels, J. Lange, Th. Schäpers, and H. Lüth, Phys. Rev. B **55**, R1958 (1997).

⁷An electro-optic modulator functions via crossed polarizers that sandwich an electrically tunable birefringent material.

⁸M. Johnson and R.H. Silsbee, Phys. Rev. Lett. **55**, 1790 (1985).

⁹M. Büttiker, Phys. Rev. Lett. **57**, 1761 (1986).

¹⁰C.W.J. Beenakker and H. van Houten, Phys. Rev. Lett. **63**, 1857 (1989).

¹¹H.X. Tang, F.G. Monzon, R. Lifshitz, M.C. Cross, and M.L. Roukes (unpublished).

¹²Among these are partial spin polarization and additional unpolar-

ized bands at E_F in **F1** and **F2**; magnetic disorder and spin scattering at the F/S interface; momentum and spin scattering in the 2DEG; and thermal smearing.

¹³Yu.V. Sharvin, Zh. Éksp. Teor. Fiz. **48**, 984 (1965) [Sov. Phys. JETP **21**, 655 (1965)].

¹⁴We assume that the $T_{ij}^{\alpha\beta}$ are essentially energy independent on the scale of the spin splitting. The latter is small compared to the Fermi energy in narrow-gap, low-density semiconductor heterostructures.

¹⁵L. D. Landau and E.M. Lifshitz, *Quantum Mechanics* (Pergamon, Oxford, 1977), pp. 471 and 472.

¹⁶J.P. Heida, B.J. van Wees, J.J. Kuipers, and T.M. Klapwijk, Phys. Rev. B **57**, 11 911 (1998).

¹⁷We find that introduction of diffuse boundary or bulk scattering to our calculations tends to wash out both the asymptotic effects and the high-field oscillations (Ref. 11). We also find that our results are insensitive to the precise formulation of the DSPR's; more complex (eight-reservoir) calculations that include junction scattering in these regions display similar physics (Ref. 11).